Acta Pharmaceutica Sinica B 2025;15(2):1056−1069

Chinese Pharmaceutical Association
Institute of Materia Medica, Chinese Academy of Medical Sciences

Acta Pharmaceutica Sinica B

www.elsevier.com/locate/apsb
www.sciencedirect.com

ORIGINAL ARTICLE

Synthesis, preclinical evaluation and pilot clinical study of a $P2Y_{12}$ receptor targeting radiotracer [^{18}F]QTFT for imaging brain disorders by visualizing anti-inflammatory microglia

Bolin Yao[a,†], Yanyan Kong[b,†], Jianing Li[a,†], Fulin Xu[c,†], Yan Deng[a], Yuncan Chen[d], Yixiu Chen[d], Jian Chen[a], Minhua Xu[e], Xiao Zhu[e], Liang Chen[d], Fang Xie[b], Xin Zhang[d,*], Cong Wang[a,f,g,*], Cong Li[a,g,*]

[a]*School of Pharmacy, MOE Key Laboratory of Smart Drug Delivery, MOE Innovative Center for New Drug Development of Immune Inflammatory Diseases, Zhongshan Hospital, Fudan University, Shanghai 201203, China*
[b]*PET Center, Department of Nuclear Medicine, Huashan Hospital, Fudan University, Shanghai 200040, China*
[c]*Department of Neurosurgery, Minhang Hospital, Fudan University, Shanghai 201199, China*
[d]*Department of Neurosurgery, Huashan Hospital, Fudan University, Shanghai 200040, China*
[e]*Department of Clinical Pharmacy and Pharmacy Administration, School of Pharmacy, Fudan University, Shanghai 201203, China*
[f]*Shanghai Key Laboratory of Molecular Imaging, Shanghai University of Medicine and Health Sciences, Shanghai 201318, China*
[g]*The Key Laboratory of Biomedical Imaging Science and System, Chinese Academy of Sciences, State Key Laboratory of Biomedical Imaging Science and System, Shenzhen 518055, China*

Received 3 October 2024; received in revised form 8 December 2024; accepted 5 January 2025

KEY WORDS

Microglia;
Neuroinflammation;
$P2Y_{12}$ receptor;

Abstract As the brain's resident immune cells, microglia perform crucial functions such as phagocytosis, neuronal network maintenance, and injury restoration by adopting various phenotypes. Dynamic imaging of these phenotypes is essential for accessing brain diseases and therapeutic responses. Although numerous probes are available for imaging pro-inflammatory microglia, no PET tracers have been developed specifically to visualize anti-inflammatory microglia. In this study, we present an ^{18}F-labeled PET

*Corresponding authors.
E-mail addresses: xinzhanghs@126.com (Xin Zhang), cong_wang@fudan.edu.cn (Cong Wang), congli@fudan.edu.cn (Cong Li).
[†]These authors made equal contributions to this work.
Peer review under the responsibility of Chinese Pharmaceutical Association and Institute of Materia Medica, Chinese Academy of Medical Sciences.

https://doi.org/10.1016/j.apsb.2025.01.009

Brain diseases;
Positron emission tomography (PET);
Epilepsy;
Aging;
Glioma

tracer (QTFT) that targets the $P2Y_{12}$, a receptor highly expressed on anti-inflammatory microglia. [^{18}F]QTFT exhibited high binding affinity to the $P2Y_{12}$ (14.43 nmol/L) and superior blood−brain barrier permeability compared to other candidates. Micro-PET imaging in IL-4-induced neuroinflammation models showed higher [^{18}F]QTFT uptake in lesions compared to the contralateral normal brain tissues. Importantly, this specific uptake could be blocked by QTFT or a $P2Y_{12}$ antagonist. Furthermore, [^{18}F]QTFT visualized brain lesions in mouse models of epilepsy, glioma, and aging by targeting the aberrantly expressed $P2Y_{12}$ in anti-inflammatory microglia. In a pilot clinical study, [^{18}F]QTFT successfully located epileptic foci, showing enhanced radioactive signals in a patient with epilepsy. Collectively, these studies suggest that [^{18}F]QTFT could serve as a valuable diagnostic tool for imaging various brain disorders by targeting $P2Y_{12}$ overexpressed in anti-inflammatory microglia.

1. Introduction

Microglia are immune cells residing intrinsically within the brain, serving as the primary defence system in the brain. They play a pivotal role in various functions, such as organizing synapses, phagocytosing pathogens, regulating neuronal excitability, clearing cellular debris, and activating innate/adaptive immunity[1]. To fulfill their diverse functions, microglia exhibit a spectrum of phenotypic polarization. The extremes of the above spectrum are categorized into pro-inflammatory microglia that fighting pathogens, and anti-inflammatory microglia that facilitating tissue repair[2]. Considering both phenotypes are actively implicated in the pathogenesis, immune microenvironment modulation, and neuroinflammation regulation, it is essential to spatially and temporally visualize the polarization states of microglia to attain a thorough comprehension of disease progression, the development of novel treatment approaches, and the assessment of therapeutic responses to potential drug candidates[3,4,5].

Positron emission tomography (PET) is well suited for imaging microglia due to its ultra-high sensitivity[6]. Several neuroinflammatory targets, including the translocator protein 18 kDa (TSPO), cyclooxygenase isoenzymes (COX), colony-stimulating factor 1 receptor (CSF1R), and purinergic receptors $P2X_7$, have been utilized to develop PET tracers aimed at visualizing pro-inflammatory microglia[7–9]. However, these tracers face limitations: (1) non-specific binding due to elevated TSPO expression in both activated astrocytes and endothelial cells; (2) the inability to distinguish between different phenotypes of activated microglia. Therefore, there is an urgent need to develop PET tracers specifically designed to visualize anti-inflammatory microglia. P2Y receptors are a class of 7-transmembrane proteins coupled to G-proteins[10]. They can be activated by extracellular signaling molecules or nucleotides released by damaged cells under conditions such as inflammation, ischemia, and hypoxia[11,12]. As a subtype of the P2Y receptors, $P2Y_{12}$ consists of 342 amino acids and is expressed on microglia in the brain parenchyma but not on vascular or meningeal macrophages[13]. Importantly, the expression of $P2Y_{12}$ on microglia is phenotypically dependent, with elevated expression in anti-inflammatory microglia[14]. The augmented $P2Y_{12}$ expression contributes to the acute inflammatory response triggered by danger-associated molecules released in brain disorders[15,16]. Notably, $P2Y_{12}$ is one of the most promising biomarkers in various challenging-to-manage diseases, including Alzheimer's disease, epilepsy, and brain tumors[17,18]. Given its specific upregulation on anti-inflammatory microglia and its sensitivity to neuroinflammation, $P2Y_{12}$ is considered an attractive target for designing radiotracers. However, effective PET tracers targeting $P2Y_{12}$ receptors within the brain are barely reported. Villa et al. reported a novel ^{11}C-piperazinyl-pyridine urea tracer[19], which targets brain lesions with high $P2Y_{12}$ expression in excised tissues from stroke mouse models and human brains. Regrettably, its limited metabolic stability and inadequate brain uptake hinder its potential for *in vivo* applications. More recently, the same group reported innovative thienopyrimidine-based PET probes designed for imaging the $P2Y_{12}$ receptor[20]. Nevertheless, these tracers are susceptible to efflux by P-glycoprotein (P-gp) within the brain. Therefore, there is a strong demand for PET tracers that are highly specific for $P2Y_{12}$ and capable of efficiently crossing the blood−brain barrier (BBB).

In this study, we synthesized four nicotinate-based radiotracers targeting $P2Y_{12}$. Among these, [^{18}F]QTFT demonstrated a high binding affinity for $P2Y_{12}$ and satisfactory BBB permeability, making it the choice for *in vivo* studies. Given the correlation between microglia activation and the progression of various brain disorders, we employed [^{18}F]QTFT to visualize brain lesions by targeting the $P2Y_{12}$-overexpressing anti-inflammatory microglia. PET imaging confirmed that this radiotracer specifically visualized IL-4-induced anti-inflammatory microglia in mouse models. Utilizing this tracer, we observed an upregulation of $P2Y_{12}$ in the acute phase of epileptic mouse models, while a down-regulation was noted in the aging mouse brain. Leveraging the accumulation of anti-inflammatory microglia in brain tumors, [^{18}F]QTFT effectively visualized orthotopic glioma allografts in mouse models, achieving a higher target-to-normal brain ratio compared to ^{18}F-fluoro-ethyl-tyrosine ([^{18}F]FET)[21], which is widely used in clinical settings to identify high-grade gliomas. Importantly, a pilot clinical study showed that [^{18}F]QTFT successfully located epileptic foci in a patient with temporal lobe epilepsy. In summary, our study validated [^{18}F]QTFT as a promising radiotracer for visualizing $P2Y_{12}$ in anti-inflammatory microglia-associated brain diseases. This PET tracer has the potential to be a valuable tool for comprehensive neuroinflammation assessment and guiding precision therapies targeting microglia.

2. Materials and methods

2.1. Reagents and materials

All solvents and reagents for the synthesis and analysis were commercially sourced without further purification unless otherwise specified. Electrospray mass spectrometry (ESI-MS) was

performed on the Agilent 1260 LC−MSD trap system (Agilent, USA). High-performance liquid chromatography (HPLC) analyses were performed on a Nexera HPLC System (Shimadzu, Japan) with a variable wavelength detector (SPD-20A, Shimadzu) and a radio-HPLC detector system (FC2000-01607) for radioactivity detection. Reverse-phase C18 column (5 μm, 250 mm × 10 mm, Agilent) for analysis process, and reverse-phase C18 column (5 μm, 250 mm × 21.2 mm, Agilent) for preparative process. NMR spectra of ^{1}H, ^{13}C, and ^{19}F were acquired using a 600 MHz Varian Gemini instrument. PET imaging of animals was conducted by SIMENS micro-PET/CT (Siemens, Germany). Clinical magnetic resonance imaging (MRI) and PET were performed using a 3T Prisma MRI system (Siemens, Germany) and a uMI780 PET-CT scanner (United Imaging, China).

2.2. Chemistry

The detailed procedures for synthesizing the corresponding compound and precursors are shown in the chemical synthesis section of the Supporting Information Briefly, precursors and standards were synthesized starting from ethyl 6-chloro-5-cyano-2-(trifluoromethyl) nicotinate or ethyl 6-chloro-5-cyano-2-(methyl) nicotinate with a 6-step process. The resulting compounds were purified by column chromatography to obtain a light-yellow oil.

2.3. General procedure for radiosynthesis of radiotracers

The preparation of aqueous fluoride 18 was obtained through $^{18}O(p,n)^{18}F$ on 95% enriched [^{18}O]H_2O with a cyclotron (GE Healthcare), and absorbed to a Sep-Pak QMA cartridge (Waters, MA, USA). This cartridge had been pretreated with 10 mL of 1.0 mol/L K_2CO_3 and 20 mL of water. The [^{18}F]Fluoride trapped on the Sep-Pak cartridge was eluted with a solution containing Kryptfix-222 (10 mg in 200 μL acetonitrile), K_2CO_3 (3.0 mg in 200 μL of ultra-pure water), acetonitrile (500 μL). The solution that was eluted was subsequently utilized for radio-fluorination. The solution was subjected to azeotropic distillation with a flow of helium, heating at 120 °C with continuous stirring until it was evaporated to dryness. Following drying, the tosylate precursor (3.0 mg) was transferred and agitated for 10 min at 120 °C while dissolved in 0.5 mL of acetonitrile. Finally, deionized water (1.0 mL) was added to the reaction and the unprocessed blend was allowed to run through a pre-activated Sep-Pak C18 cartridge and further washed with deionized water (10 mL). After being eluted with 1.0 mL of methanol, the radioactive products that were still in the solid phase were subjected to HPLC using an Inertsil® ODS-4 GL Science, Inc., Tokyo column. The mobile phase employed a gradient program: 0 min, 60% B; 15 min, 40% B; 30 min, 0% B; 40 min, 0% B; flow rate: 2 mL/min; A phase: MeCN; B phase: water with 0.1% TFA.

2.4. Determination of lipophilicity

The lipophilicity was tested through the classical method. Briefly, the mixture of *n*-octanol (600 μL) and PBS (pH 7.4, 600 μL) was mixed with radiotracers (10 μL, 185 kBq), and shaken for 30 min violently. Subsequently, the mixture was allowed to be kept in the centrifuge for 3 min at 2000 rpm. The organic phase and aqueous phase were separated, and the radioactivity of each phase (100 μL) was measured using a γ-counter (PerkinElmer; Waltham, MA, USA). The log$D_{7.4}$ values were calculated and the experiments were performed in triplicate.

2.5. In vitro and in vivo stability

In vitro stability was studied in saline and serum. Briefly, a freshly prepared solution of [^{18}F]TFT/[^{18}F]QTFT (10 μL) was mixed with saline or mouse serum (100 μL; Abcam Inc., MA, USA) and incubated with agitation (500 rpm) at 37 °C. At 0.5, 2 and 4 h, 30 μL aliquots from these mixtures were mixed with an equal volume of MeCN. After vigorous stirring on a vortex mixer, the samples were subsequently centrifuged (2655×*g* for 3 min, Thermo, USA) to precipitate serum proteins. Finally, a portion of the supernatant was subjected to radio-HPLC analysis.

In vivo stability was studied in healthy mice, and blood was harvested and analysed by radio-HPLC. In the initial, healthy mice were anesthetized with isoflurane, and intravenously injected with [^{18}F]QTFT (11.1 MBq) *via* tail vein. Then, the whole blood collected from tail vein at 60 and 120 min were centrifugated at 10,621×*g* (Thermo, USA) for 10 min after precipitated with cold acetonitrile. The supernatant was separated and analysed with radio-HPLC.

2.6. Molecular docking

The docking assay for TFT/QTFT was performed against human $P2Y_{12}$ (PDB: 4PXZ) by using the Schrödinger suit for protein and ligand preparation, optimizing 3D structures with pH = 7.0. Energy minimization was performed using the semiempirical quantum mechanical method. All of the water molecules and the ligands were removed by PyMOL, and executed image optimization. The active site of TFT/QTFT against $P2Y_{12}$ was delineated based on the AZD1283 binding site. The ligands were then inserted into the workspace for docking. The docking process implements a high efficient grid-based docking algorithm, thoroughly exploring the binding site's free volume. Through the optimization of the ligand and incremental construction, the conformational space of various ligands against protein was measured. The final results were ranked based on the lowest interaction energy values, which encompassed van der Waals interactions, hydrogen hydrophobic interactions, and hydrogen bond interactions.

2.7. Cell uptake

Rat C6 glioma cells and bEnd.3 cells were unfrozed and then cultured in a medium containing DMEM with 10% FBS. Cells were maintained in a humidified atmosphere of 5% CO_2 and 95% air at 37 °C. At the time of the experiment, cells in standard condition were digested and re-cultured in a 24-well plate with 500 μL of the culture DMEM overnight. On the following day, the medium was replaced with 300 μL of [^{18}F]QTFT/[^{18}F]TFT (20 GBq/μmol) and 50 μL of serum-free DMEM. Then, the mixture was transferred to an atmosphere of 5% CO_2 at 37 °C for 5, 15, 30, 60 and 90 min. Inhibition experiments were performed by adding an excess unlabeled QTFT/TFT (50 μg). After incubation, the medium was removed and successively washed with cold PBS. Finally, cells were digested with 0.5 mol/L NaOH and collected for gamma counting.

2.8. Transwell assay

The mouse microvascular endothelial cell line bEnd.3 was seeded on the upper side of the 0.4 μm Transwell insert filters with a density of 1 × 10^4 cells/well in a 12-well cell culture

plate. The models could be applied once the *trans*-endothelial cell electrical resistance (TEER) values of the bEnd.3 cell monolayer reached 1000 Ω cm^2. PBS medium containing [^{18}F]TFT/[^{18}F]QTFT (0.37 MBq) was added into the well for incubation. The medium in the lower chamber was collected and counted with a gamma counter. The inhibition experiments were conducted by administering the P-glycoprotein (P-gp) inhibitor verapamil (1.0 μg) 30 min prior to the incubation with [^{18}F]TFT or [^{18}F]QTFT (0.37 MBq). The medium in the lower chamber was collected and counted with a gamma counter.

2.9. *In vitro binding assays*

The affinities of [^{18}F]TFT and [^{18}F]QTFT binding to $P2Y_{12}$ were measured using the rat C6 glioma cell line expressing $P2Y_{12}$. The C6 cell line was maintained in DMEM with 10% FBS in flasks. Before the binding assay, media was replaced only with DMEM and digested with trypsinization, and cells were suspended in saline for binding assay. About 1×10^5 cells per well were incubated with various concentrations of the purified [^{18}F]TFT/[^{18}F]QTFT ranging from 0.1 to 50 nmol/L and contained for 60 min at 37 °C. The incubation was halted by dilution with pre-cooled saline (0.5 mL) and cells were centrifugated at 2000 rpm for 2 min. Unbound radioactivity was washed from cell pellets with cold saline, and collected by centrifugation to obtain supernatants. The total bound of the radioactivity of cell precipitate and the unbound educt were quantified using a gamma counter. Non-specific binding was determined by co-culturing with pre-fabricated 100-fold equivalent unlabelled TFT/QTFT. Through subtracting the non-specific bound radioactivity from the radio-activity of the total binding, specific binding could be calculated.

2.10. *Animal models*

Normal C57BL/6 mice (male, 18−22 g) were purchased from SLAC of Shanghai. Animal studies of all were executed following the guidelines of the Chinese Committee of Management of Laboratory Animals, and were authorized by the Ethics Committee of Fudan University School of Pharmacy. The approval number is 2019-03-FY-LC-01.

IL-4/LPS-induced anti-/pro-inflammatory mouse models and epilepsy mouse models were constructed through the reported method. Briefly, the mice were anesthetized constantly with a flow of isoflurane (rate: 0.4 L/min, concentration: 1.5%) in the entire procedure. The skulls of mice were exposed while the preparation of transferring mice to the stereotactic fixation instrument was completed. Each mouse underwent a small hole drilled as previously reported work[22]. The inducing medications of 1 μL, namely (IL-4, 100 ng), (LPS, 1 μg), (KA, 0.3 μg) were injected with a 1.0-μL Hamilton syringe and stitched up after injection. The control group was dealt with the identical method with the same volume of saline. After injection of KA or saline, the behaviour was monitored, and EEG performance was also measured and recorded. The acute epilepsy models went through a status epilepticus with a duration of at least 30 min. Then, the mice were picked out for EEG and subsequent PET imaging 48−72 h post-operation. The chronic epilepsy models of recurrent 7−8 days post-SE were monitored and picked out for EEG recording and subsequent PET imaging.

In situ glioma mouse models were constructed through the reported method. Briefly, the mice were anesthetized constantly with a flow of isoflurane (rate: 0.4 L/min, concentration: 1.5%) in the entire procedure. The skulls of mice were exposed while the preparation of transferring mice to the stereotactic fixation instrument was completed. Each mouse underwent small hole drilled as previous reported work[23]. The mouse glioma cells were prepared in advance and diluted to a 5 μL suspension (1×10^5 cells/μL). 1 μL of the cell suspension were extracted and injected with a 1.0-μL Hamilton syringe. The control group were dealt with the identical method with a same volume of PBS. After injection 10 days, the mice were monitored the tumour with MRI, and verified with a clinical diagnosis PET medicine, [^{18}F]FET (11.1 MBq).

2.11. *Micro-PET/CT imaging*

Micro-PET/CT scan was conducted with SIEMENS Inveon scanner. The normal mice or disease models were anesthetized with isoflurane, and intravenously injected with [^{18}F]TFT/[^{18}F]QTFT (11.1 MBq) *via* tail vein. Micro PET/CT images were obtained at 30, 60, 90 and 120 min as 10-min static images or as dynamic scans of 60-min following the administration of [^{18}F]TFT/[^{18}F]QTFT. For the blocking experiment, static scan of mice at 30, 60, 90 and 120 min were performed after the co-injection of [^{18}F]TFT/[^{18}F]QTFT (11.1 MBq) with 1.0 mg/kg Clopidogrel or QTFT per animal. In the analysis of the results of PET images, the regions of interest were quantified by SIMENS Inveon Research Workplace software (V3.0, Siemens, Germany). The regions of interest were quantified by manually on the target regions. The radio-activities of regions of interest were converted and normalized as the standard uptake value (SUV). The radios of target to normal were computed by dividing the radio-activities of the VOIs in the contralateral normal brain.

2.12. *Pharmacokinetics*

The whole blood was collected from the mice that had been administered [^{18}F]TFT/[^{18}F]QTFT (11.1 MBq) *via* tail vein at 1, 5, 15, 30, 60 and 120 min. Successively, the samples were weighted and determined using a gamma counter. Pharmacokinetic parameters were then calculated and analysed using NONMEM (nonlinear mixed-effects modelling, V7.5) and FOCE-I for estimation. R Foundation for Statistical Computing (V4.1.1) and the R packages (V1.2.0) were used for analysing statistics and visualisation of consequence. As the change in lipophilicity and polarity may affect the PK behaviour of the tracer, the PK model was used to the comparison of TFT and modified probes QTFT. PK models of one to three compartments were analysed. The model was on the basis of GOF plots, OFV, AIC, and VPC.

2.13. *Biodistribution study*

The biodistributions was conducted in normal C57BL/6 mouse ($n = 3$−6 at each time point; body weight 20−25 g). Mice were injected through the tail vein with 100 μL of the radiotracer (11.1 MBq) dissolved in saline containing 10% ethanol. Animals were anesthetized and sacrificed at the set time, subsequently, tissues were separated, weighted, and analysed for radioactivity. The proportion of the injected dose per gram was computed by calculating the counts of tissues.

2.14. *Clinical trial*

The clinical study was approved by the Ethics Committee of Huashan Hospital (NO. KY2024-713). All volunteers provided

written informed consent. Dynamic PET imaging of [^{18}F]QTFT for 90 min was conducted in volunteers on a uMI780 PET-CT scanner. The volumes of interest (VOIs) were then drawn and mensurated in PMOD (V4.4, Switzerland) to calculate the standardized uptake values (SUVs) of the lesion and the contralateral. Time-activity curve (TAC) of the corresponding region was also generated by PMOD from 0 to 90 min.

2.15. *Statistical analysis*

Statistical analysis was carried out with GraphPad Prism (V7.0, GraphPad Software, USA). Data were expressed as mean ± standard deviation (SD). We used a Student's *t*-test (two-tailed) and a one-way analysis of variance (ANOVA) for comparisons. Not significant (ns), $*P < 0.05$, $**P < 0.01$, $***P < 0.001$, and $****P < 0.0001$. $P < 0.05$ was considered statistically significant. The curves were fitted using a one-site binding model with a sum-of-squares *F* test for *Ki*.

3. Results

3.1. *Synthesis and characterization of radiotracers [^{18}F]TFT and [^{18}F]QTFT*

The synthetic routes for four P2Y$_{12}$ ligands are illustrated in Fig. 1. These precursors were synthesized from ethyl 6-chloro-5-cyano-2-(trifluoromethyl) nicotinate or ethyl 6-chloro-5-cyano-2-methylnicotinate in a total of 5 steps, achieving an overall chemical yield of 37%−41% (Fig. 1A). Non-labelled standards were also synthesized for confirming the correct product formation in radiosynthesis, with chemical yields varying from 6% to 15% (Fig. 1B). Details of the synthesis can be found in the Supporting Information Figs. S1 and S2. The BBB permeability of a PET radiotracer is usually influenced by biochemical characteristics such as topological polar surface area (TPSA), size, lipophilicity, pK_a, hydrogen bonding, plasma protein binding, and efflux transporters. Therefore, the chemical parameters of four synthetic tracers, TFT, TMT, QTFT and QTMT, were investigated (Table 1). Low TPSA and high lipophilicity values suggest that QTFT and TFT may be candidates for high BBB permeability.

Utilizing computer-aided design to analyse the docking mode of ligands with the receptor protein provides valuable insights into the structure−function relationship. The docking score represents a computational binding energy of ligand-protein. The low docking scores observed for QTFT and TFT make them promising candidates for further radio-evaluation (Fig. 2A and B). Similar molecular docking modes of TFT and QTFT with P2Y$_{12}$ indicated the two types of tracers may have similar pharmacological characteristics. [^{18}F]TFT and [^{18}F]QTFT were synthesized using a typical nucleophilic fluorination process, taking approximately 90 min in total. The final products were confirmed by the non-radioactive TFT/QTFT (Supporting Information Fig. S3), and obtained radiochemical purities (RCP) of greater than 95% after purification *via* HPLC. The decay-corrected radiochemical yield (RCY) was determined to be 9.9 ± 1.5% and 10.3 ± 1.1%, with molar activity ranging from 80 to 120 GBq/μmol. *In vitro* stability of [^{18}F]TFT/[^{18}F]QTFT was determined by radio-HPLC (Fig. 2C and D and Supporting Information Fig. S4), and the results

Table 1 Biochemical parameters of P2Y$_{12}$ ligands.

Ligand	TPSA	*C*Log*P*	Log$D_{7.4}$	Docking score
TFT	128.93	2.21	1.54 ± 0.92	−10.280
QTFT	86	3.1	2.08 ± 0.65	−10.410
TMT	128.93	1.81	0.99 ± 1.62	−9.642
QTMT	86	2.69	1.11 ± 1.02	−9.907

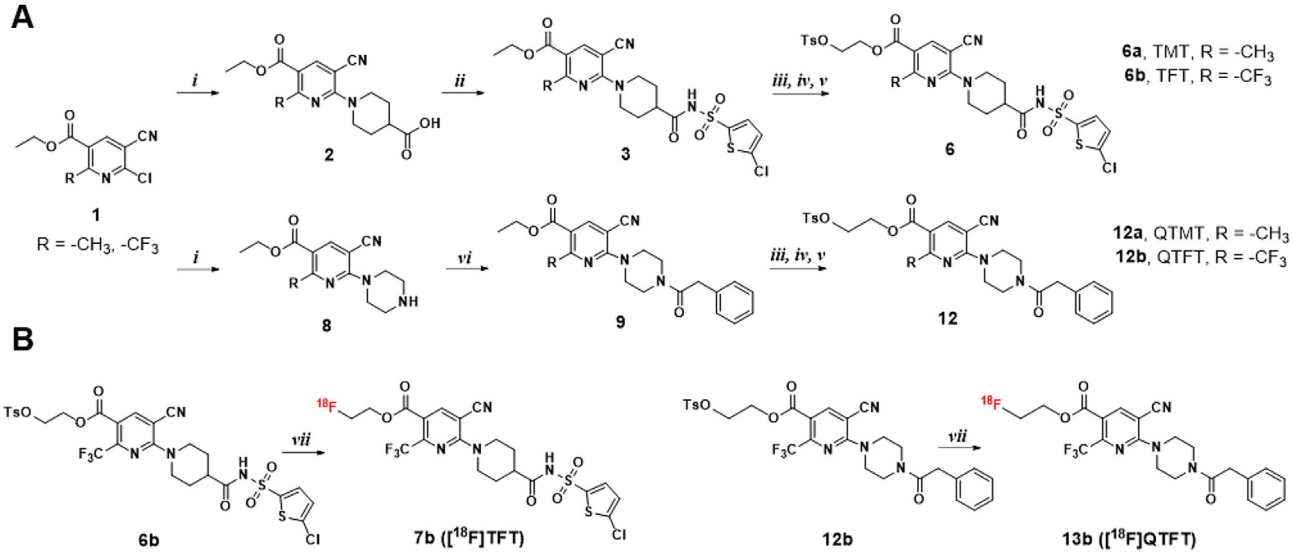

Figure 1 Synthesis of P2Y$_{12}$ targeting radiotracers. (A) Synthetic procedure of intermediates TMT, TFT, QTMT, and QTFT. (i) 3-Azetidinecarboxylic acid, DIPEA, EtOH, 60 °C, 1 h; (ii) 5-Chlorothiophene-2-sulfonamide, EDC, HOBT, DIPEA, DCM, 0° to R.T., 24 h; (iii) LiOH (1.0 M), THF, water, R.T., 3 h; ethanol, 50 °C, 12 h; (iv) Ethylene glycol, EDC, DMAP, DCM, 0 °C to R.T., 5 h; (v) Tosyl chloride, DMAP, pyridine, 0 °C to R.T., 3 h; (vi) Piperazine, DIPEA, EtOH, 60 °C, 1 h. (B) Radiosynthesis of [^{18}F]TFT and [^{18}F]QTFT. (vii) $^{18}F^-$, K2.2.2, K_2CO_3, MeCN, 10 min.

revealed no radio decompositions until 4 h after incubation with saline and serum. Additionally, the *in vivo* stability of [^{18}F]QTFT was investigated using radio-HPLC (Fig. 2E). The results indicated that the tracer exhibited robust stability, with no notable release of free ^{18}F or metabolites detected within 2 h in mice.

3.2. *P2Y$_{12}$ affinity and BBB permeability studies of radiotracers*

The binding affinity of [^{18}F]TFT and [^{18}F]QTFT to the P2Y$_{12}$ receptor was assessed using a membrane-binding assay, demonstrating that both tracers exhibit a strong affinity for P2Y$_{12}$ (Fig. 3A). Specifically, the dissociation constant (K_d) of [^{18}F]TFT was 6.55 nmol/L, while that of [^{18}F]QTFT was 14.43 nmol/L. The time-dependent cellular uptakes of [^{18}F]TFT and [^{18}F]QTFT were studied in a P2Y$_{12}$-positive C6 glioblastoma cell line. The results showed that the cellular uptakes of [^{18}F]TFT and [^{18}F]QTFT increased with incubation time. Additionally, cellular uptakes were significantly decreased upon the introduction of excess P2Y$_{12}$ inhibitor clopidogrel (Fig. 3B). To be effective for brain disease imaging, radiotracers must efficiently cross the BBB and not be pumped out by P-glycoprotein (P-gp). The BBB permeabilities of [^{18}F]TFT and [^{18}F]QTFT were evaluated using a Transwell assay by culturing mouse brain endothelial bEnd.3 cells in the apical compartment[24,25] (Fig. 3C). The endothelial transmission value of [^{18}F]QTFT reached 19.6%, while that of [^{18}F]TFT was only 7.5%, indicating the superior BBB penetration of [^{18}F]QTFT (Fig. 3D). The transmembrane transport of [^{18}F]TFT and [^{18}F]QTFT across a bEnd.3 cell monolayer was further assessed using a Transwell assay in the presence of P-gp inhibitor verapamil. Notably, the presence of verapamil resulted in a remarkable increase in [^{18}F]TFT penetration efficacy to 17.2%, while the efficacy of [^{18}F]QTFT only slightly increased to 21.5% (Fig. 3D). These results indicate that P-gp blockade significantly increases the transmembrane amount of [^{18}F]TFT, while showing minimal effect on [^{18}F]QTFT, suggesting that [^{18}F]QTFT is not a substrate for P-gp. These studies imply that [^{18}F]QTFT achieves effective BBB penetration and targets brain P2Y$_{12}$ by overcoming P-gp-mediated cellular efflux.

3.3. *PET imaging and pharmacokinetics analysis of [^{18}F]TFT and [^{18}F]QTFT in vivo*

The brain pharmacokinetics of [^{18}F]TFT and [^{18}F]QTFT in healthy mice were investigated using a micro-PET/CT imaging, and the two tracers exhibited differences in brain uptake (Fig. 4A and B). Both radiotracers exhibited high liver uptake and intestine accumulation, possibly owing to their high lipophilicity (Supporting Information Table S1). In comparison to [^{18}F]TFT, [^{18}F]QTFT demonstrated higher brain penetration and accumulation (Fig. 4C). The peak of SUV of [^{18}F]QTFT reached 1.77 ± 0.27, almost double that of [^{18}F]TFT (0.44 ± 0.34). The retention level of [^{18}F]QTFT was SUVmean = 0.69 ± 0.11, while [^{18}F]TFT only reached 0.12 ± 0.08. The dynamic PET results indicated that [^{18}F]QTFT surpassed [^{18}F]TFT in terms of BBB penetrability and brain uptake. *Ex vivo* pharmacokinetic study revealed that [^{18}F]QTFT and [^{18}F]TFT exhibited a rapid blood clearance with a half-life of

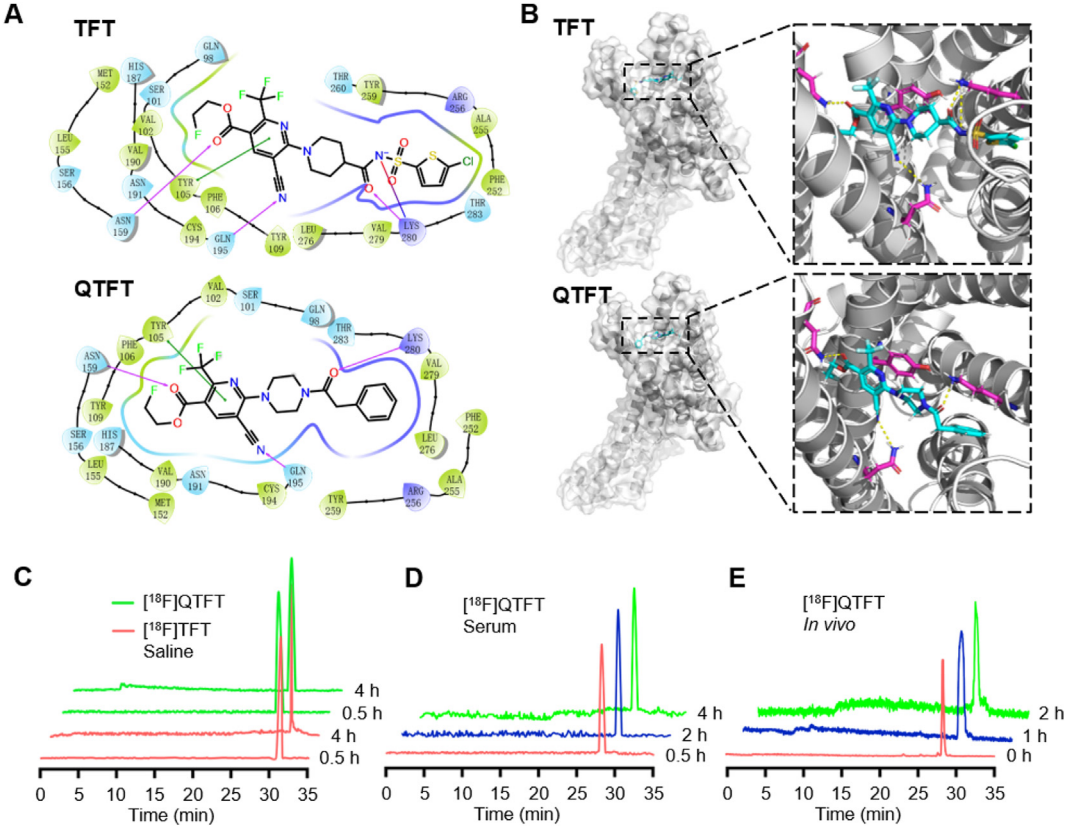

Figure 2 [^{18}F]TFT and [^{18}F]QTFT show high metabolic stability. (A) 2D binding modes of TFT and QTFT. (B) The co−crystal structure of TFT and QTFT bound to P2Y$_{12}$ receptor (PDB ID code 4PXZ). (C) *In vitro* stability of [^{18}F]QTFT and [^{18}F]TFT in saline. (D) *In vitro* stability of [^{18}F]QTFT in isolated mouse serum. (E) *In vivo* stability of [^{18}F]QTFT in blood stream.

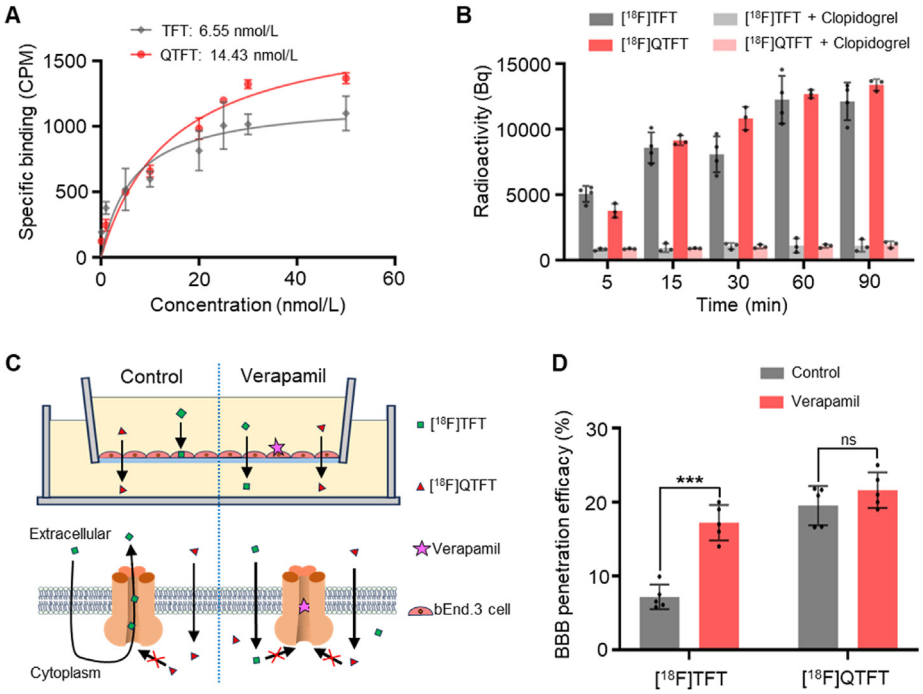

Figure 3 [^{18}F]QTFT shows high BBB permeability and binding affinity for P2Y$_{12}$. (A) Saturation binding assays using P2Y$_{12}$ over-expressing C6 glioblastoma cancer cells show dissociation constants for [^{18}F]TFT (K_d = 6.55 nmol/L) and [^{18}F]QTFT (K_d = 14.43 nmol/L). (B) Time-dependent C6 cell uptakes of [^{18}F]TFT and [^{18}F]QTFT in presence and absence of clopidogrel. (C) A schematic interprets the strategy evaluating BBB permeability of [^{18}F]TFT and [^{18}F]QTFT in an *in vitro* Transwell system. P-gp expressed on the membrane of brain capillary endothelial cells actively pumps out of its substrate [^{18}F]TFT, but not [^{18}F]QTFT. (D) The BBB penetration efficacies of [^{18}F]TFT and [^{18}F]QTFT in the presence or absence of verapamil were evaluated by using *in vitro* Transwell system. The data are shown as mean ± SD, n = 3−6. $P > 0.05$ (ns), ***$P < 0.001$.

30.57 and 27.14 min, respectively (Supporting Information Fig. S5), reflecting a comparable behaviour of these two probes. Furthermore, we validated *in vivo* specificity of [^{18}F]QTFT to P2Y$_{12}$ receptors. Following the blockade of QTFT, the SUV of [^{18}F]QTFT in brain tissue decreased by 72.3% (Fig. 4B and D). Considering that the inherently low P2Y$_{12}$ expression levels in healthy mouse brains may impact blocking efficacy, we conducted the competitive studies in mouse models bearing subcutaneous C6 glioma model with elevated P2Y$_{12}$ expression[26]. The uptake of [^{18}F]QTFT in the subcutaneous tumors was significantly inhibited by P2Y$_{12}$ inhibitor clopidogrel (72.8%, Supporting Information Fig. S6). Consequently, we selected [^{18}F]QTFT, which exhibits higher brain penetration and specific P2Y$_{12}$ binding properties, for subsequent imaging studies.

3.4. [^{18}F]QTFT visualizes activated microglia in IL-4-induced neuroinflammation-mouse models

To confirm the P2Y$_{12}$ targeting specificity of [^{18}F]QTFT, inflammatory mouse models induced by IL-4 and LPS were developed. The LPS-induced group did not exhibit any apparent signal change in the brain, whereas the IL-4-induced group demonstrated a rising signal within the IL-4-induced lesion but not in the contralateral region. After being blocked with P2Y$_{12}$ inhibitor clopidogrel (1.0 mg/kg), a decreased PET signal by approximately 1.45-fold was observed, indicating high specificity and low non-specific binding of [^{18}F]QTFT (Fig. 5A and B). Tissue samples from the LPS-induced pro-inflammatory region and the IL-4-induced anti-inflammatory region were collected for immunohistochemical staining, the higher expression of P2Y$_{12}$ in the IL-4-administered region further confirmed that [^{18}F]QTFT could image anti-inflammatory microglia (Fig. 5C and D).

3.5. [^{18}F]QTFT locates epileptic foci in the acute stage of KA-induced epilepsy models

Reactive microglia have been reported to exhibit a variety of functional phenotypes during epileptogenesis. The epileptic mouse models were established through hippocampal injection of kainic acid, and the electroencephalogram (EEG) was recorded after the corresponding epilepsy stage (the acute: 1−3 days after status epilepticus (SE)); the latent: 8−20 days after SE; the chronic: 20−180 days after SE) (Fig. 6A and B and Supporting Information Fig. S7). As shown in Fig. 6C, [^{18}F]QTFT PET showed a high signal in the ipsilateral hippocampus of epilepsy mouse models during the acute phase (*T/N* ratio = 1.81 ± 0.22 at 60 min p.i.). Conversely, [^{18}F]QTFT PET in latent and chronic epilepsy mouse models showed relatively low accumulation in brain lesions (*T/N* ratio = 1.14 ± 0.05 and 1.12 ± 0.03) (Fig. 6D). Nissl staining revealed a significant loss of neurons during the acute phase of epilepsy, with a slight increase in the chronic phase (Fig. 6E and F). Immunohistochemical staining of the epileptic tissues demonstrated the upregulation of P2Y$_{12}$ in the acute phase, but not in the chronic phase (Fig. 6E and G).

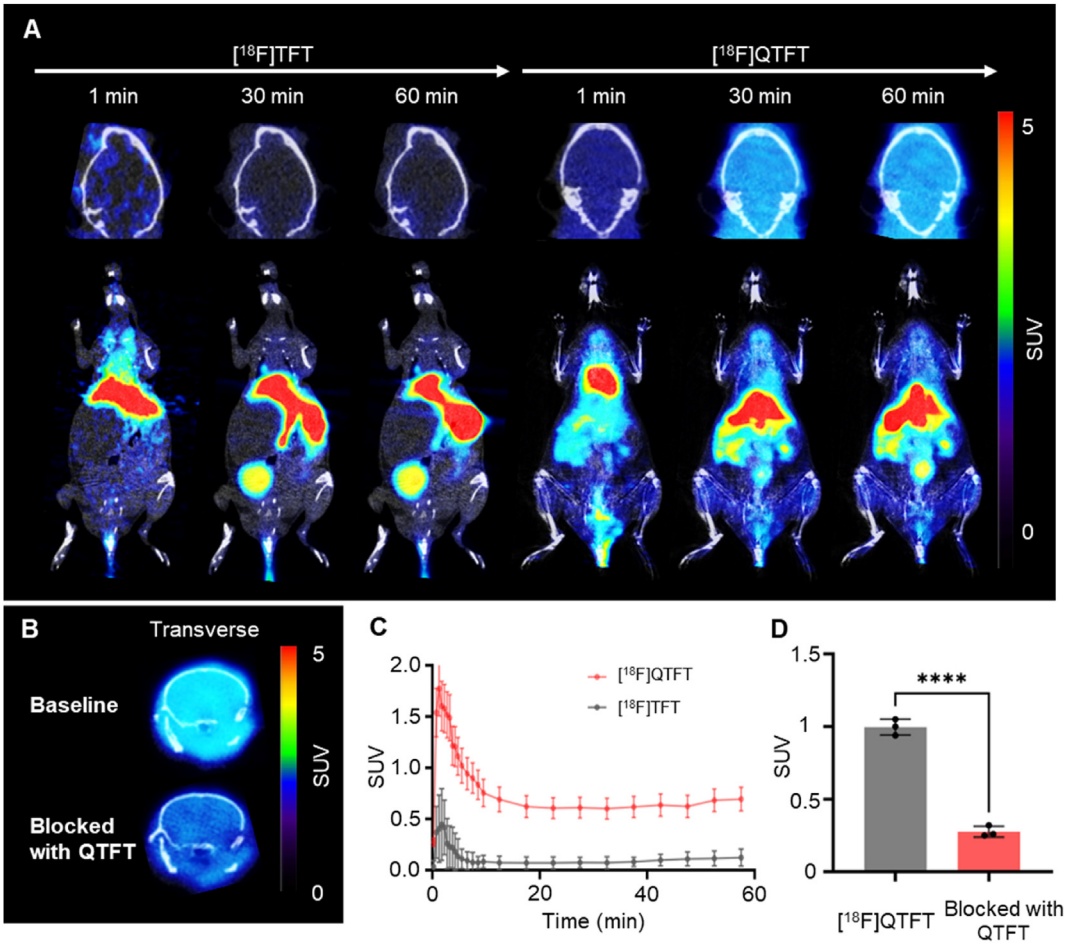

Figure 4 [^{18}F]QTFT shows higher brain uptake than [^{18}F]TFT. (A) Representative dynamic PET/CT images of healthy C57BL/6 mice administrated with 18.5 MBq of $P2Y_{12}$ radiotracer [^{18}F]TFT and [^{18}F]QTFT. (B) Representative PET/CT images of normal C57BL/6 mouse brain at 60 min post administration of 3.7 MBq [^{18}F]QTFT alone or the [^{18}F]QTFT that was blocked by QTFT. (C) Time-activity curves (TACs) of brain uptake of normal C57BL/6 mice administrated with [^{18}F]TFT and [^{18}F]QTFT. (D) Brain uptake of normal C57BL/6 mice at 60 min post administrated with [^{18}F]QTFT alone or pre-blocked with QTFT. The data are shown as mean ± SD, $n = 3$. ****$P < 0.0001$.

3.6. [^{18}F]QTFT shows down-regulated $P2Y_{12}$ expression in aging mouse brains

Aging is one of the greatest risk factors in the etiology of neurodegenerative diseases. Therefore, understanding the spatiotemporal dynamics of microglial transformation with aging is crucial for the prevention or treatment of age-related diseases. To visualize the discrepancy of $P2Y_{12}$ expression of microglia in aging mice, we conducted dynamic PET/CT imaging analysis on 60- and 40-week aging mouse models compared with 6-week young mouse models. As shown in Fig. 7A and B, [^{18}F]QTFT PET exhibited a higher uptake in the brain of young mouse models, reaching a peak SUV of 2.01 ± 0.31 at 1.25 min (compared to 1.96 ± 0.18 and 0.98 ± 0.19 in 40- and 60-week aging brain). The retention level of the 40- and 60-week aging is 0.52 ± 0.04 and 0.45 ± 0.06 at 60 min respectively, which is remarkably lower than that of 0.61 ± 0.06 observed in the young mice. These results suggests that the decrease in $P2Y_{12}$ expression during the aging can be visualized by [^{18}F]QTFT. Immunohistochemical staining of the brain tissues also revealed decreased $P2Y_{12}$ expression in the aged brain (Fig. 7C and Supporting Information Fig. S8).

3.7. [^{18}F]QTFT defines the glioma allograft in mouse models

The immunosuppressive microenvironment of gliomas, the most common malignant brain tumour in adults, is closely linked to the anti-inflammatory transformation of microglia. Anti-inflammatory microglia can produce growth factors, which enhance glioma cell proliferation, reduce glioma cell apoptosis, and promote tumour cell migration. Therefore, PET imaging of anti-inflammatory microglia will facilitate the localization of brain gliomas and the assessment of immunotherapy. We first established a glioma mouse model by intracranial injection of GL261 cells and confirmed tumour formation using T2-weighted MRI (Fig. 8A and B). Subsequently, we imaged the gliomas with [^{18}F]QTFT and compared it to the amino acid metabolism imaging agent [^{18}F]FET. The results showed that [^{18}F]QTFT exhibited a higher target-to-normal ratio in tumour detection compared to [^{18}F]FET. The T/N ratio of [^{18}F]QTFT was 1.47 ± 0.01, higher than that of [^{18}F]FET (1.17 ± 0.02) (Fig. 8C). Immunofluorescence staining further confirmed that [^{18}F]QTFT specifically imaged $P2Y_{12}$-expressing microglia (Fig. 8D and Supporting Information Fig. S9).

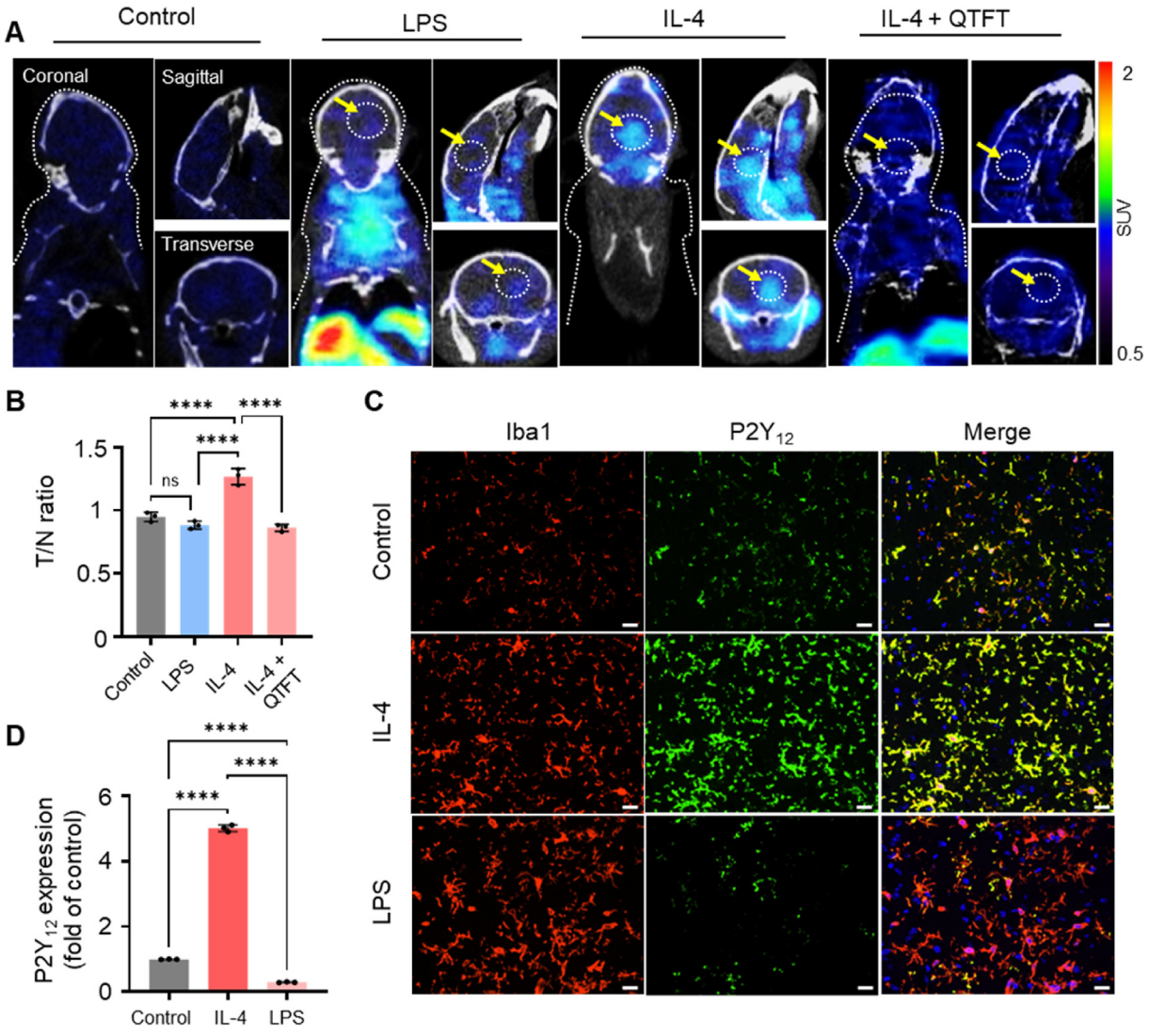

Figure 5 [^{18}F]QTFT visualizes brain lesions with microglia polarized into anti-inflammatory phenotypes. (A) Representative PET/CT images of LPS-/IL-4-induced mouse models at 60 min after administration of 3.7 MBq of [^{18}F]QTFT or blocked with $P2Y_{12}$ inhibitors. (B) The *T*/*N* ratios of [^{18}F]QTFT in PBS (control), LPS, IL-4 and IL-4/QTFT blockade treated brain tissue. (C) Confocal fluorescence microscopic images of mouse brain tissues treated with PBS (control), IL-4, or LPS. The immune-fluorescence of $P2Y_{12}$ and Iba1 was displayed in green and red respectively. DAPI fluorescence was displayed in blue. (D) Quantification of the $P2Y_{12}$ expression level in brain tissues treated with PBS, IL-4 or LPS (fold of control). The data are shown as mean ± SD, $n = 3$. $P > 0.05$ (ns), $^{****}P < 0.0001$. Scale bar = 20 μm.

3.8. Pilot clinical trial of [^{18}F]QTFT in patients with epilepsy

To further evaluate the translational potential, we conducted [^{18}F]QTFT PET imaging in a patient with temporal lobe epilepsy. A detectable lesion in the right temporal lobe was observed on T2 weighted MR images (Fig. 9A). Then [^{18}F]FMZ PET imaging revealed a negative signal in the lesion area (epileptic focus SUVmean = 0.54 ± 0.28) compared to the contralateral normal brain (SUV_{mean} = 5.45 ± 0.35). Subsequently, dynamic [^{18}F]QTFT PET imaging showed high signal intensity in the epileptic focus (Fig. 9B, Supporting Information Figs. S10 and S11). Quantitative analysis indicated an SUVmean of 1.29 ± 0.28 in the epileptic focus, whereas the contralateral normal brain region had an SUVmean of 0.90 ± 0.16. As shown in Fig. 9B, [^{18}F]QTFT demonstrated high BBB permeability with a peak SUV of 2.50 ± 1.58 in the lesion and 2.19 ± 1.42 in the contralateral normal region. These results suggested that [^{18}F]QTFT held promise for locating the epileptic foci in epilepsy patients.

4. Discussion

$P2Y_{12}$, a G protein-coupled purinergic receptor, is activated by adenosine diphosphate or adenosine triphosphate[11]. In the peripheral system, $P2Y_{12}$ activation triggers platelet aggregation and thrombus formation. Due to its robust antiplatelet and antithrombotic effects, $P2Y_{12}$ antagonists are commonly used to treat cardiovascular diseases[13]. Recent studies have unveiled that $P2Y_{12}$ receptors are also expressed in brain microglial cells, where they play a role in synaptic plasticity and neuroinflammation[14]. Following anti-inflammatory initiation in the central nervous system, $P2Y_{12}$ receptor expression rapidly

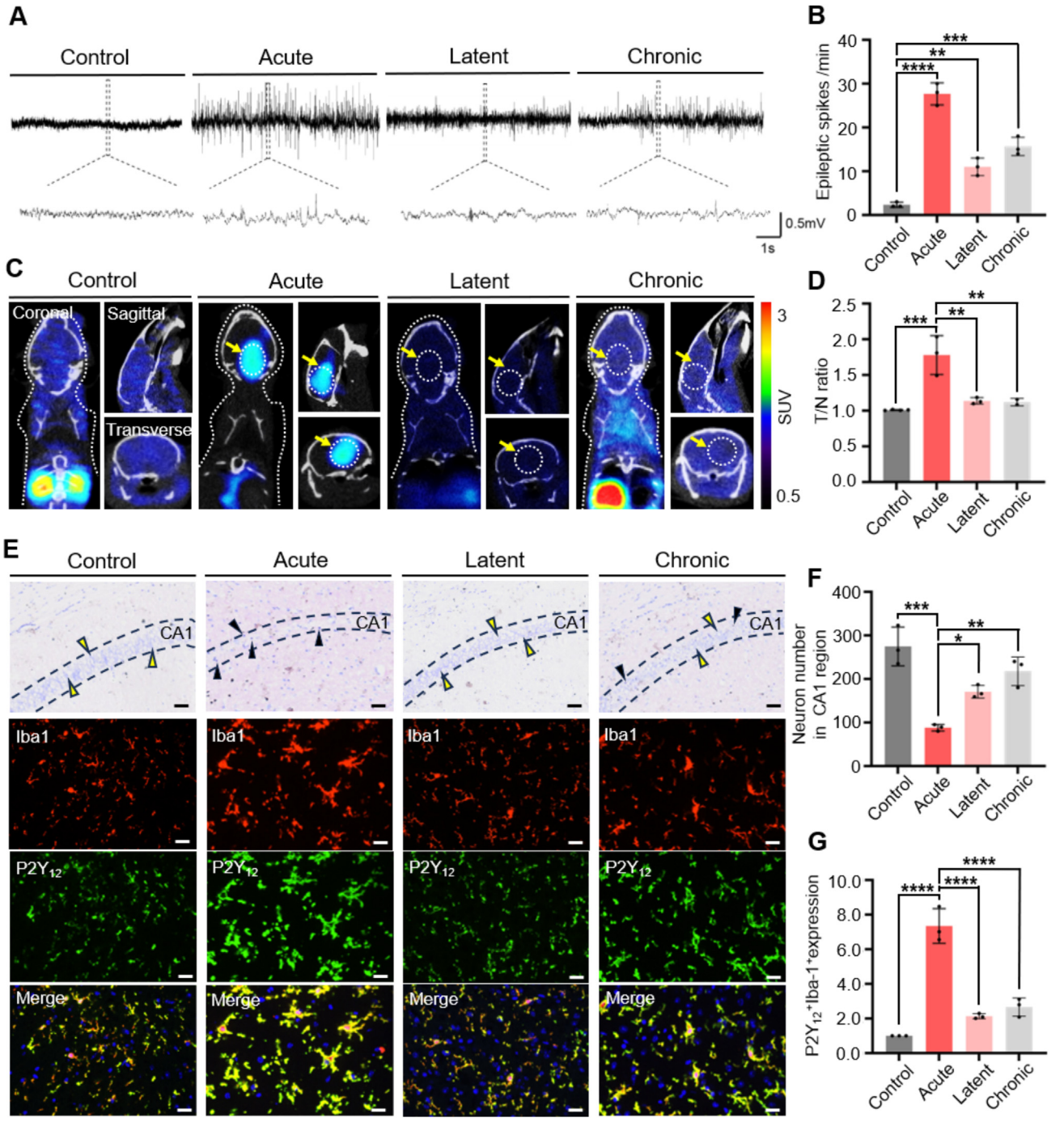

Figure 6 [^{18}F]QTFT visualizes epileptic foci by locating anti-inflammatory microglia. (A) Representative electroencephalogram of epileptic models at the acute, latent and chronic stages. The healthy mice were used as controls. (B) The number of epileptic spikes in the epileptic models at the acute, latent and chronic stages. (C) Representative PET/CT images of the acute and chronic epilepsy mouse models at 60 min after administration of 3.7 MBq of [^{18}F]QTFT. (D) *T/N* ratios of the animal models treated with PBS (control), and at the acute, latent and chronic stages of epilepsy. (E) Immunohistochemical and immunofluorescence staining of the control brain tissue and epileptic tissues at acute, latent or chronic stages. (F) Quantification of the neuron number in the CA1 region. (G) The cells with both $P2Y_{12}$ and Iba1 positive expression (fold of control). The immune-fluorescence of $P2Y_{12}$ and Iba1 was displayed in green and red respectively. DAPI fluorescence was displayed in blue. The data are shown as mean ± SD, $n = 3$. $^{*}P < 0.05$, $^{**}P < 0.01$, $^{***}P < 0.001$ and $^{****}P < 0.0001$. In the Nissl staining, scale bar = 35 μm. In the immunofluorescence staining, scale bar = 20 μm.

increases, leading to microglial activation and significant chemotactic responses[16]. These observations suggest that $P2Y_{12}$ could serve as an ideal biomarker for distinguishing anti-inflammatory microglial cells.

In this study, we synthesized a series of $P2Y_{12}$-specific radiotracers by using $P2Y_{12}$ receptor inhibitor AZD1283 as a prototype[27]. We retained the crucial binding unit, the nicotinate group, along with the hydrogen bond acceptor present in

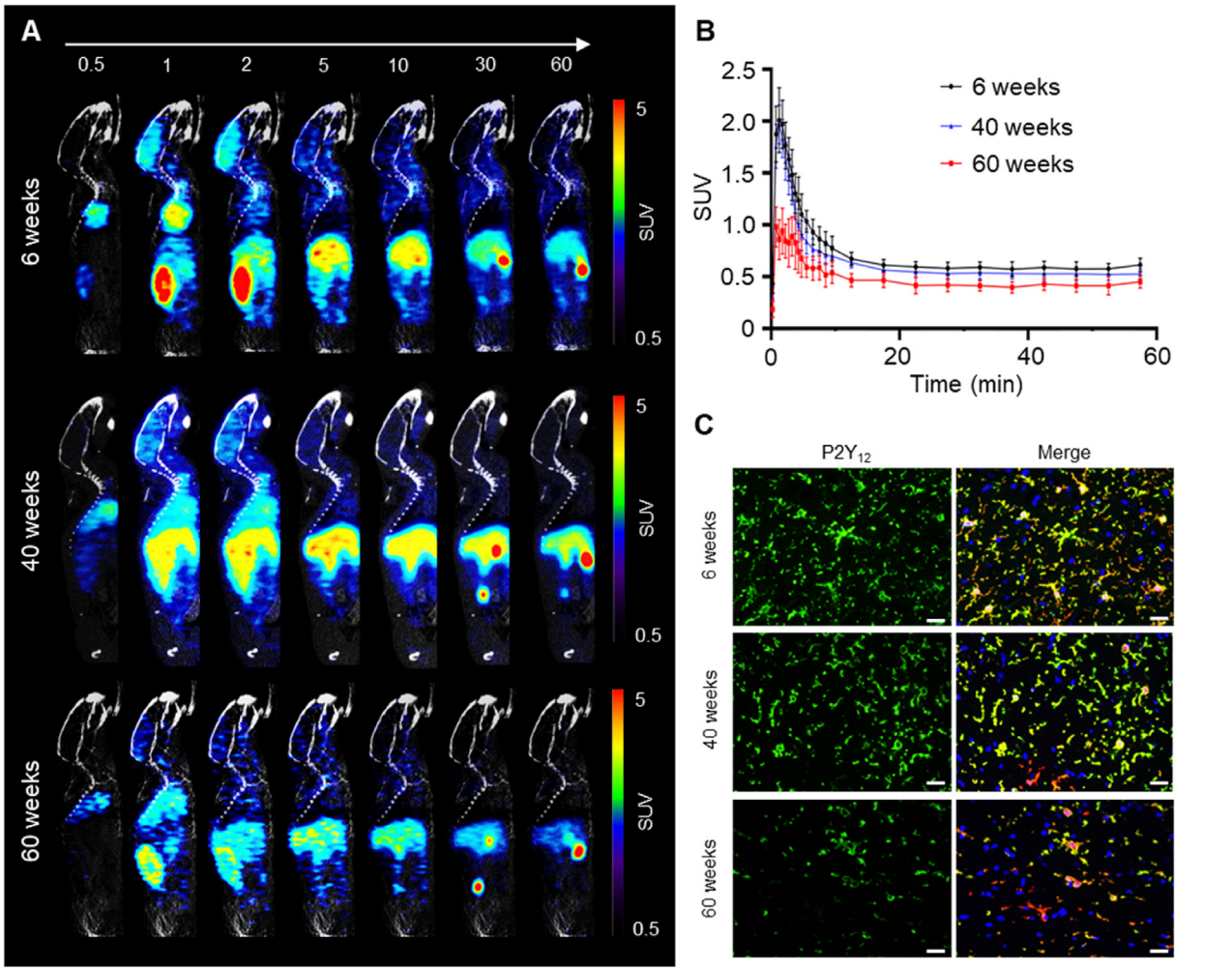

Figure 7 [^{18}F]QTFT shows a decrease in anti-inflammatory microglia in aged mouse brains. (A) Representative dynamic PET/CT images of aging mice (60 and 40 weeks) and the young (6 weeks) administrated with 11.1 MBq of [^{18}F]QTFT. (B) Time−activity curves (TACs) of brain uptake of [^{18}F]QTFT in the aging and young mice. (C) Representative images of the $P2Y_{12}$ immunofluorescence staining of microglia from young and aging mice brain samples. The immune-fluorescence of $P2Y_{12}$ and Iba1 was displayed in green and red respectively. DAPI fluorescence was displayed in blue. The data are shown as mean ± SD, $n = 3$. Scale bar = 20 μm.

AZD1283. These components interact with Tyr105 and Lys280 of the $P2Y_{12}$ receptor through hydrophobic or $\pi-\pi$ stacking interactions. Additionally, we introduced sulfamide groups and amide groups to enhance lipophilicity. After evaluating the lipophilicity, receptor affinity and BBB penetration of the compounds, we selected TFT and QTFT for radiolabeling with fluorine 18. Notably, the receptor targeting affinity of [^{18}F]QTFT can be blocked by the $P2Y_{12}$ receptor inhibitor clopidogrel, confirming the specificity of this radiotracer to $P2Y_{12}$ receptor. Subsequently, *in vitro* Transwell experiments confirmed the superior BBB-crossing properties of QTFT compared to TFT. In addition, P-gp efflux assays indicated that QTFT was not a substrate for P-gp. The most likely due to the replacement of the sulfamide groups with benzylamide, which reduces molecular polarity and decreases the compound's tendency to interact with P-gp residues. To our best knowledge[17,19,20], this study presents the first $P2Y_{12}$ targeted PET tracer specifically designed for *in vivo* imaging of anti-inflammatory microglia.

Microglia polarized to different phenotypes play intricate roles in brain disorders[28]. Numerous compounds have been developed to inhibit (*e.g.*, minocycline) or clear (*e.g.*, PLX5622) activated microglia. However, due to the coexistence of different phenotypes in epileptogenesis, indiscriminate therapeutic methods to clear or suppress activated microglia may lead to ineffective treatments or even worsen the condition[29]. In this study, utilizing [^{18}F]QTFT PET imaging, we reveal an increase in the anti-inflammatory microglia during the acute phase of epileptic mouse models. This finding suggests that microglia may exert neuroprotective effects during the early stages of epilepsy[30]. In addition, epilepsy surgery is considered the most effective method for achieving long-term seizure freedom, particularly in patients with drug-resistant epilepsy[31]. Accurate localization of the epileptogenic focus is crucial for the surgical treatment of refractory epilepsy. Clinically, localization of the epileptogenic focus can be defined by [^{18}F]FMZ based on the downregulation of GABA-A receptors in lesions. However, the negative signal indicated by [^{18}F]FMZ usually suffers from compromised sensitivity and specificity. In this study, we showed the feasibility to identify epileptic foci using [^{18}F]QTFT PET in a patient with temporal lobe epilepsy. Compared with [^{18}F]FMZ

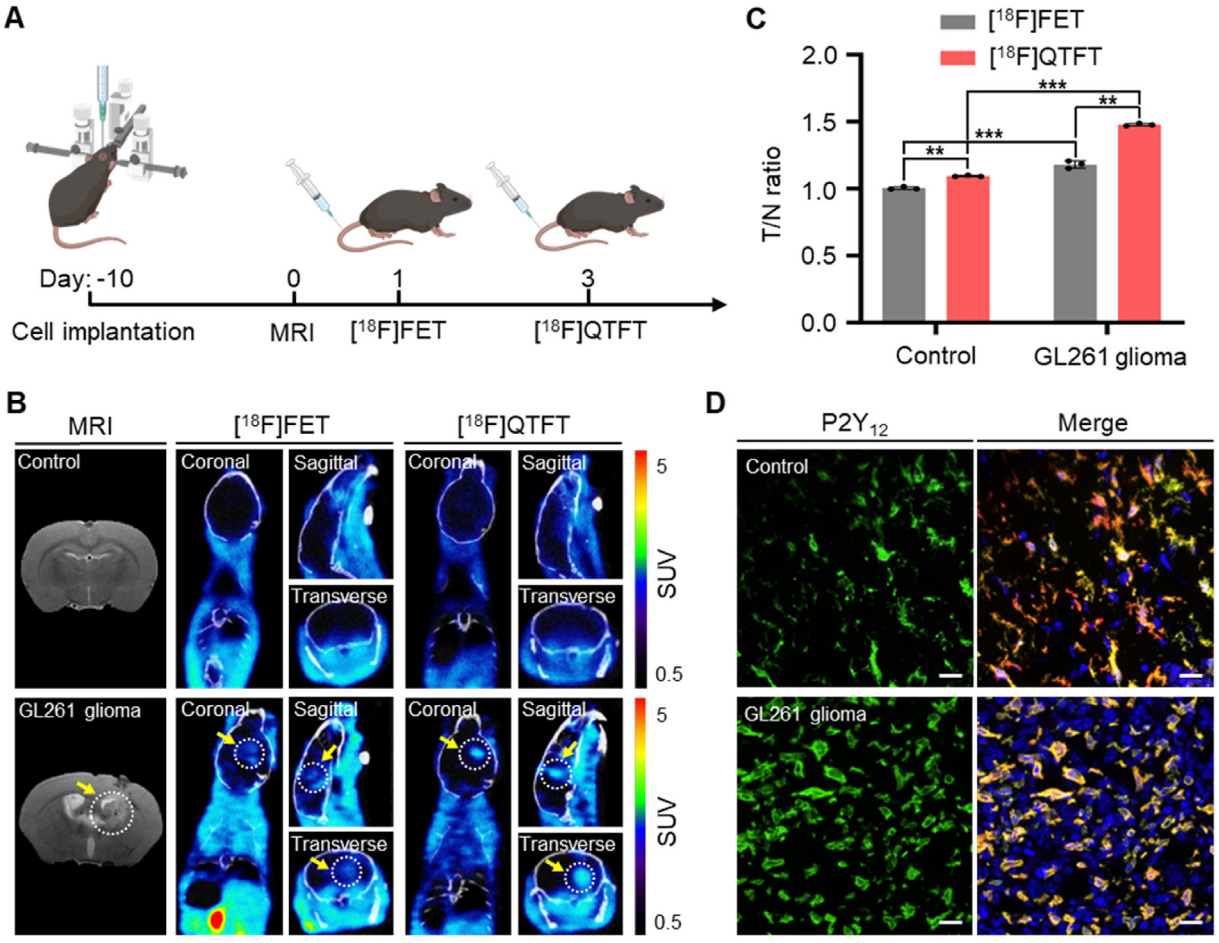

Figure 8 [^{18}F]QTFT visualizes orthotopic glioma allograft in mouse models. (A) The procedure in developing and imaging glioma models with PET tracers of [^{18}F]FET followed [^{18}F]QTFT. (B) Representative MRI and PET/CT images of the same mouse model after intravenous administration of [^{18}F]FET followed [^{18}F]QTFT. (C) *T/N* ratios of GL261 glioma allograft measured from the PET images post injection of [^{18}F]FET or [^{18}F]QTFT. (D) Immunofluorescence staining of the normal brain and tumor tissues. The immune-fluorescence of $P2Y_{12}$ and Iba1 was displayed in green and red respectively. DAPI fluorescence was displayed in blue. The data are shown as mean ± SD, $n = 3$. $^{**}P < 0.01$ and $^{***}P < 0.001$. Scale bar = 20 μm.

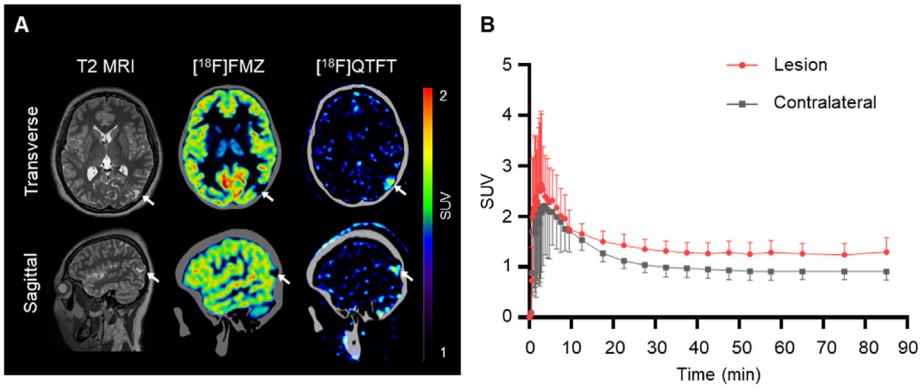

Figure 9 [^{18}F]QTFT imaging epileptic foci in an epileptic patient. (A) [^{18}F]QTFT PET imaging of a temporal lobe epilepsy patient at 90 min post intravenous administration. T2-weighted MR imaging and[^{18}F]FMZ imaging confirm the location of epileptic foci. (B) Time-activity curves (TACs) of the epileptic lesion and contralateral normal brain after the administration of [^{18}F]QTFT. The data are shown as mean ± SD.

PET, [^{18}F]QTFT showed a positive signal in the epileptogenic focus, making identification more convenient. Therefore, [^{18}F]QTFT holds promise for positive imaging of the epileptogenic focus and revealing the spatiotemporal dynamics of anti-inflammatory microglia during epilepsy progression.

Low-grade neuroinflammation is a common feature of the aging brain, evidenced by microglia activation[32]. As the brain ages, microglia can become senescent, adopting a pro-inflammatory phenotype that exacerbates neuroinflammation, reduces phagocytic activity and imparts neuroprotective functions. These changes contribute to cognitive decline and neurodegenerative diseases. However, the role of anti-inflammatory macroglia in the aging brain is not well understood. In this work, we observed a substantial decrease in $P2Y_{12}$ levels in the brains of aging mice. This suggests that [^{18}F]QTFT could be a valuable tool for exploring the complex interactions between microglial phenotypes and aging, highlighting the phenotypic plasticity of microglia as they shift between pro-inflammatory and anti-inflammatory states in response to aging.

Glioma is the most common and aggressive primary brain tumour in adults. Its limited response to immunotherapies is largely due to the suppressive tumour immune microenvironment, characterized by a high abundance of tumour-associated macrophages/microglia. These cells contribute to glioma invasion, angiogenesis, and immunosuppression, making them critical therapeutic targets[33]. Radiotracers like [^{18}F]FET have been applied clinically to image glioma because they are actively taken up by highly metabolic glioma cells[34]. However, these tracers cannot evaluate the glioma-associated inflammatory response or immune microenvironment. In this study, we developed [^{18}F]QTFT, a tracer that effectively visualizes microglia activation in glioma-transplanted mice. Compared to [^{18}F]FET, [^{18}F]QTFT offers higher contrast in tumor localization. This tracer provides a valuable tool for locating malignant brain tumor, accessing early treatment response assessments, planning therapeutic strategies, and designing clinical trials.

This study has several limitations. High tracer uptake in the liver and off-target binding may increase the risk of radiation exposure, underscoring the necessity for further optimization of the probe's structure to minimize non-target uptake while preserving its effectiveness in visualizing anti-inflammatory microglia in the brain. Moreover, our research concentrated exclusively on epilepsy, glioma, and specific stages of aging, without addressing different phases of disease progression. Future investigations will aim to assess the probe's imaging capabilities across a broader spectrum of neuroinflammation-related brain disorders and investigate its potential for clinical applications.

5. Conclusions

In this work, we synthesize and screen a PET probe, [^{18}F]QTFT, tailored for specific imaging of $P2Y_{12}$ receptors. The tracer exhibits an impressive capability to circumvent P-gp-mediated efflux and traverse the BBB, enabling quantitative imaging of $P2Y_{12}$ expression on microglia across a diverse range of preclinical mouse models and clinical patients of neuroinflammatory diseases. Further clinical studies are essential to determine the tracer's applicability in a range of neuroinflammatory brain disorders, including neurodegenerative diseases and cerebrovascular conditions.

Acknowledgments

This study was supported by the National Key Research and Development Program of China (2023YFA1801200), the National Natural Science Foundation of China (92159304, 82202224, 82227806, 82030049, 823B1003, 81971666, 82204544, 82472038), the National Science Fund for Distinguished Young Scholars (82025019, China), the Construction Project of Shanghai Key Laboratory of Molecular Imaging (18DZ2260400, China), the Shanghai Rising Star Program (23QA1407700, China), the Shanghai Explorer Program (23TS1401100, China), and the 2020 Fund Project of Shanghai Health Committee (202040106, China), the open fund of National Key Laboratory of Advanced Drug Formulations for Overcoming Delivery Barriers.

Author contributions

Study conception and design: Cong Li and Cong Wang. Experiment construction and implementation: Bolin Yao, Yanyan Kong, Jianing Li, Fulin Xu, Yan Deng, Yuncan Chen, Yixiu Chen and Minhua Xu. Data acquisition and processing: Bolin Yao, Yanyan Kong, Jianing Li, Yan Deng, Yuncan Chen, Yixiu Chen, Jian Chen, Xiao Zhu, Liang Chen, Fang Xie and Xin Zhang. Writing of Manuscript: Cong Wang and Cong Li. Supervision and coordination of the study: Cong Wang and Cong Li. All authors commented on previous versions of the manuscript. All authors read and approved the final manuscript.

Conflicts of interest

The authors have no conflicts of interest to declare.

Appendix A. Supplementary information

Supporting information to this article can be found online at https://doi.org/10.1016/j.apsb.2025.01.009.

References

1. Borst K, Dumas AA, Prinz M. Microglia: immune and non-immune functions. *Immunity* 2021;**54**:2194–208.
2. Paolicelli RC, Sierra A, Stevens B, Tremblay ME, Aguzzi A, Ajami B, et al. Microglia states and nomenclature: a field at its crossroads. *Neuron* 2022;**110**:3458–83.
3. Duan WJ, Wang C, Jiang YQ, Sui A, Li Z, Wang L, et al. A ratiometric SERS probe for imaging the macrophage phenotypes in live mice with epilepsy and brain tumor. *Adv Healthc Mater* 2023;**12**:e2301000.
4. Fan DD, Yue Q, Chen J, Wang C, Yu RL, Jin ZY, et al. Reprogramming the immunosuppressive microenvironment of *IDH1* wild-type glioblastoma by blocking *Wnt* signaling between microglia and cancer cells. *Oncoimmunology* 2021;**10**:e1932061.
5. Zhang WL, Chen HQ, Ding LY, Huang J, Zhang MR, Liu Y, et al. Microglial targeted therapy relieves cognitive impairment caused by *Cntnap4* deficiency. *Exploration* 2022;**3**:20220160.
6. Jain P, Chaney AM, Carlson ML, Jackson IM, Rao A, James ML. Neuroinflammation PET imaging: current opinion and future directions. *J Nucl Med* 2020;**61**:1107–12.
7. Kreisl WC, Kim MJ, Coughlin JM, Henter ID, Owen DR, Innis RB. PET imaging of neuroinflammation in neurological disorders. *Lancet Neurol* 2020;**19**:940–50.

8. Fu WH, Lin QY, Yang TT, Shi D, Shi HC, Cheng DF, et al. Synthesis and evaluation of TSPO-targeting radioligand [18F]F-TFQC for PET neuroimaging in epileptic rats. *Acta Pharm Sin B* 2024;**14**: 2211−3835.
9. Shukuri M, Mawatari A, Takatani S, Tahara T, Inoue M, Arakaki W, et al. Synthesis and preclinical evaluation of ^{18}F-labeled ketoprofen methyl esters for cyclooxygenase-1 imaging in neuroinflammation. *J Nucl Med* 2022;**63**:1761−7.
10. Kolb HC, Barret O, Bhattacharya A, Chen G, Constantinescu C, Huang CF, et al. Preclinical evaluation and nonhuman primate receptor occupancy study of ^{18}F-JNJ-64413739, a PET radioligand for $P2X_7$ receptors. *J Nucl Med* 2019;**60**:1154−9.
11. Burnstock G. Introduction to purinergic Signalling in the brain. *Adv Exp Med Biol* 2020;**1202**:1−12.
12. Yuan SG, Chan HCS, Vogel H, Filipek S, Stevens RC, Palczewski K. The molecular mechanism of $P2Y_1$ receptor activation. *Angew Chem-int Edit* 2016;**55**:10331−5.
13. Zhang KH, Zhang J, Gao ZG, Zhang DD, Zhu L, Han GW, et al. Structure of the human $P2Y_{12}$ receptor in complex with an antithrombotic drug. *Nature* 2014;**509**:115−8.
14. Moore CS, Ase AR, Kinsara A, Rao VTS, Michell-Robinson M, Leong SY, et al. $P2Y_{12}$ expression and function in alternatively activated human microglia. *Neurol-Neuroimmunol Neuroinflammation* 2015;**2**:e80.
15. Mildner A, Huang H, Radke J, Stenzel W, Priller J. $P2Y_{12}$ receptor is expressed on human microglia under physiological conditions throughout development and is sensitive to neuroinflammatory diseases. *Glia* 2017;**65**:375−87.
16. Gu N, Eyo UB, Murugan M, Peng JY, Matta S, Dong HL, et al. Microglial $P2Y_{12}$ receptors regulate microglial activation and surveillance during neuropathic pain. *Brain Behav Immun* 2016;**55**:82−92.
17. Maeda J, Minamihisamatsu T, Shimojo M, Zhou XY, Ono M, Matsuba Y, et al. Distinct microglial response against Alzheimer's amyloid and tau pathologies characterized by $P2Y_{12}$ receptor. *Brain Commun* 2021;**3**:fcab011.
18. Beaino W, Janssen B, Kooij G, van der Pol SM, van Het Hof B, van Horssen J, et al. Purinergic receptors $P2Y_{12}$R and $P2X_7$R: potential targets for PET imaging of microglia phenotypes in multiple sclerosis. *J Neuroinflamm* 2017;**14**:259.
19. Van der Wildt B, Janssen B, Pekošak A, Stéen EJL, Schuit RC, Kooijman EJM, et al. Novel thienopyrimidine-based PET tracers for $P2Y_{12}$ receptor imaging in the brain. *ACS Chem Neurosci* 2021;**12**: 4465−74.
20. Villa A, Klein B, Janssen B, Pedragosa J, Pepe G, Zinnhardt B, et al. Identification of new molecular targets for PET imaging of the microglial anti-inflammatory activation state. *Theranostics* 2018;**8**: 5400−18.
21. Richard MA, Fouquet JP, Lebel R, Lepage M. Determination of an optimal pharmacokinetic model of ^{18}F-FET for quantitative applications in rat brain tumors. *J Nucl Med* 2017;**58**:1278−84.
22. Liu M, Jiang LJ, Wen M, Ke Y, Tong XZ. Microglia depletion exacerbates acute seizures and hippocampal neuronal degeneration in mouse models of epilepsy. *Am J Physiol-Cell Physiol* 2020;**319**: C605−10.
23. Wang C, Zhang JP, Song SL, Li Z, Yin SJ, Duan WJ, et al. Imaging epileptic foci in mouse models a low-density lipoprotein receptor-related protein-1 targeting strategy. *Ebiomedicine* 2021;**63**:103156.
24. Gao XH, Qian J, Zheng SY, Changyi YZ, Zhang JP, Ju SH, et al. Overcoming the blood-brain barrier for delivering drugs into the brain by using adenosine receptor nanoagonist. *ACS Nano* 2014;**8**:3678−89.
25. Park JS, Choe K, Khan A, Jo MH, Park HY, Kang MH, et al. Establishing co-culture blood-brain barrier models for different neurodegeneration conditions to understand its effect on BBB integrity. *Int J Mol Sci* 2023;**24**:5283.
26. Wypych D, Barańska J. Cross-talk in nucleotide signaling in glioma C6 cells. *Adv Exp Med Biol* 2020;**1202**:35−65.
27. Janssen B, Vugts DJ, Funke U, Molenaar GT, Kruijer PS, Dollé F, et al. Synthesis of the first carbon-11 labelled $P2Y_{12}$ receptor antagonist for PET imaging of microglial activation in neuroinflammation. *J Labelled Compd Rad* 2015;**58**:17.
28. Salter M, Stevens B. Microglia emerge as central players in brain disease. *Nat Med* 2017;**23**:1018−27.
29. Kinoshita S, Koyama R. Pro- and anti-epileptic roles of microglia. *Neural Regen Res* 2021;**16**:1369−71.
30. Yu C, Deng XJ, Xu D. Microglia in epilepsy. *Neurobiol Dis* 2023;**185**: 106249.
31. Wang C, Sun WB, Zhang J, Zhang JP, Guo QH, Zhou XY, et al. An electric-field-responsive paramagnetic contrast agent enhances the visualization of epileptic foci in mouse models of drug-resistant epilepsy. *Nat Biomed Eng* 2021;**5**:278−89.
32. Wendimu MY, Hooks SB. Microglia phenotypes in aging and neurodegenerative diseases. *Cells* 2022;**11**:2091.
33. Winkeler A, Boisgard R, Awde AR, Dubois A, Thézé B, Zheng JZ, et al. The translocator protein ligand [^{18}F]DPA-714 images glioma and activated microglia in vivo. *Eur J Nucl Med Mol Imaging* 2012;**39**: 811−23.
34. Maurer GD, Bruker DP, Stoffels G, Filipski K, Filss CP, Mottaghy FM, et al. ^{18}F-FET PET imaging in differentiating glioma progression from treatment-related changes: a single-center experience. *J Nucl Med* 2020;**61**:505−11.